Multi-color background-free coherent anti-Stokes Raman scattering microscopy using a time-lens source

YIFAN QIN,[1,2,3] BO LI,[2,4] FEI XIA,[2] YUANQIN XIA,[1] AND CHRIS XU[2]

[1]National Key Laboratory of Science and Technology on Tunable Laser, Harbin Institute of Technology, Harbin 150080, China
[2]School of Applied and Engineering Physics, Cornell University, Ithaca, NY 14853, USA
[3]yq88@cornell.edu
[4]bl627@cornell.edu

Abstract: We demonstrate a multi-color background-free coherent anti-Stokes Raman scattering (CARS) imaging system, using a robust, all-fiber, low-cost, multi-wavelength time-lens source. The time-lens source generates picosecond pulse trains at three different wavelengths. The first is 1064.3 nm, the second is tunable between 1052 nm and 1055 nm, and the third is tunable between 1040 nm and 1050 nm. When the time-lens source is synchronized with a mode-locked Ti:Sa laser, two of the three wavelengths are used to detect different Raman frequencies for two-color on-resonance imaging, whereas the third wavelength is used to obtain the off-resonance image for nonresonant background subtraction. Mixed poly(methyl methacrylate) (PMMA) and polystyrene (PS) beads are used to demonstrate two-color background-free CARS imaging. The synchronized multi-wavelength time-lens source enables pixel-to-pixel wavelength-switching. We demonstrate simultaneous two-color CARS imaging of CH_2 and CH_3 stretching vibration modes with real-time background subtraction in *ex vivo* mouse tissue.

1. Introduction

Coherent Raman scattering (CRS) microscopy, with contrast from coherent anti-Stokes Raman scattering (CARS) [1,2] or stimulated Raman scattering (SRS) [3], is a valuable imaging technique that overcomes some of the limitations of spontaneous Raman microscopy. It allows label-free and chemically specific imaging of biological samples with endogenous image contrast based on vibrational spectroscopy.

There are several requirements in realizing CRS imaging, and a critical one is the temporal synchronization of two picosecond excitation sources, which provide the pump and Stokes fields. The wavelength difference between the two excitation sources must match the molecular vibrational frequency of interest, and the spectral bandwidths of the sources should be narrower than the relevant Raman resonance linewidth. Several schemes have been used to meet the requirements of CRS imaging. Two picosecond mode-locked Ti:Sa lasers were applied in [4,5], and the synchronization was realized with a phase-locked-loop (PLL) and fine cavity adjustments. The signal and idler beams from a picosecond synchronously pumped optical parametric oscillator (OPO) were also used as excitation sources for CRS imaging [6]. However, synchronized mode-locked lasers and OPOs are costly and environmentally sensitive, with the need of precise alignment and careful maintenance [7]. Sources based on optical fiber technology are capable of overcoming some of these limitations, and several concepts have been demonstrated. However, a robust, energetic, and low-cost excitation source remains a major challenge for CRS imaging. For example, the power of super-continuum generation and soliton self-frequency shift is insufficient [8–11], the imaging speed of unseeded four-wave mixing is limited [12], and the realization of fiber-based OPO is challenging [13].

The existence of nonresonant background, which is a major drawback of CARS, could distort or even overwhelm resonant signal of Raman peaks, reducing the image contrast. Although SRS signal does not contain nonresonant background, it can be affected by cross phase modulation, transient-absorption, and photo-thermal effects, which will also reduce image contrast [14]. CARS signal is generated at a new wavelength, which will avoid influence of these pump-probe backgrounds. Multiple methods have been used to suppress or eliminate nonresonant background in order to retrieve pure Raman responses, including polarization-sensitive detection [15], time-resolved detection [16], frequency modulation [17,18], and nonlinear interferometric vibrational imaging [19]. These techniques are limited by either resonant signal attenuation or complicated implementation. A simple and efficient method has been applied in [20,21] to remove nonresonant background by digitally subtracting the off-resonance image from the on-resonance image. This is the technique that we will explore further in this work.

Recently, we demonstrated synchronized picosecond light sources for CRS imaging based on the time-lens concept [22–25]. A time-lens applies temporal quadratic phase modulation on a continuous wave (CW) laser, and thus broadens its spectral bandwidth [26–33], and it can be implemented conveniently with fiber-integrated electro-optic phase modulators. As the input radio-frequency (RF) for the phase modulation is derived from a mode-locked laser, synchronized picosecond pulses can be generated with proper dispersion compensation. The capability of synchronization with any mode-locked laser is the most appealing advantage of the time-lens source, apart from other benefits such as robust all-fiber configuration, picosecond pulse width, and high peak power. Moreover, electronic tuning of the pulse delay is used to achieve temporal overlap between the pump and Stokes pulse trains for CRS imaging, eliminating the need of cumbersome mechanical optical delay lines.

In this paper, we demonstrate a robust, cost-effective, all-fiber, multi-wavelength time-lens source for multi-color background-free CARS imaging. The time-lens source generates picosecond pulse trains at three different wavelengths: 1064.3 nm, between 1052 nm and 1055 nm, and between 1040 nm and 1050 nm. All three pulse trains are synchronized with a mode-locked Ti:Sa laser. We used two of the three wavelengths for two-color on-resonance imaging, and the third wavelength for off-resonance imaging and nonresonant background subtraction. We demonstrate the capability of the multi-wavelength time-lens source by performing simultaneous two-color CARS imaging of CH_2 and CH_3 stretching vibration modes with real-time nonresonant background subtraction.

2. Experimental results

The experimental setup (Fig. 1) can be divided into three parts, the pump, the Stokes (time-lens source), and the microscope. Through a pulse shaper with a slit, 100 fs pulses from a mode-locked Ti:Sa laser (Mai Tai HP DeepSee, Spectra-Physics) are broadened to ~1 ps, serving as the pump for CARS imaging. The slit is mounted on a stage to tune the wavelength of the spectrally filtered beam.

A time-lens source is synchronized with the Ti:Sa laser (pump), serving as the Stokes. A GaAs photodetector (ET-4000, EOT) converts the 80 MHz optical pulse train from the Ti:Sa mode-locked laser to a RF pulse train. The RF pulse train is then divided into two branches by an RF divider. One branch is filtered by a narrowband filter centered at the 125th harmonic of the 80 MHz repetition rate, with a 3 dB bandwidth of 50 MHz. The resulting 10 GHz sinusoid is amplified to ~14 V_{pp} to drive two electro-optic phase modulators (2PMs, EOSPACE). The other branch is amplified by a broadband amplifier to drive a Mach-Zehnder intensity modulator (IM, EOSPACE). A wavelength-tunable (1051.5-1055.5 nm) DFB-CW laser (DFB-1054-PM-50, Innolume), a wavelength-stabilized (1064.3 nm) FBG-CW laser (QFBGLD-1060-30p, QPhotonics), and a wavelength-tunable (1040-1075 nm) CW laser (TEC-520-1060-80, Sacher Lasertechnik) are, respectively, the sources for the three wavelength channels, CH1, CH2 and CH3, of the time-lens source. The channels are

combined by a wavelength division multiplexer (WDM). After phase modulation by the two PMs, the IM carves synchronized pulses onto the combined CW lights. Due to the limited bandwidth of the electrical components, the resulting pulses have temporal width of 80 ps (full-width-at-half-maximum, FWHM). Two pre-amps (home-made Yb^{3+} doped fiber amplifiers) are used to compensate for the power loss of the PMs and IM. All aforementioned fiber components of the time-lens source are polarization-maintaining, which provide enhanced power and environmental stability. A power amp (home-made Yb^{3+} doped fiber amplifier) boosts the power of the time-lens source to approximately 1 W. A transmission grating pair is used for dispersion compensation and pulse compression. The length and dispersion of the optical fiber (mostly in the pre-amp and the power amp after the IM) causes fixed walk-offs among the pulses of the three channels, which are compensated by adjusting the positions of the three mirrors in the compressor.
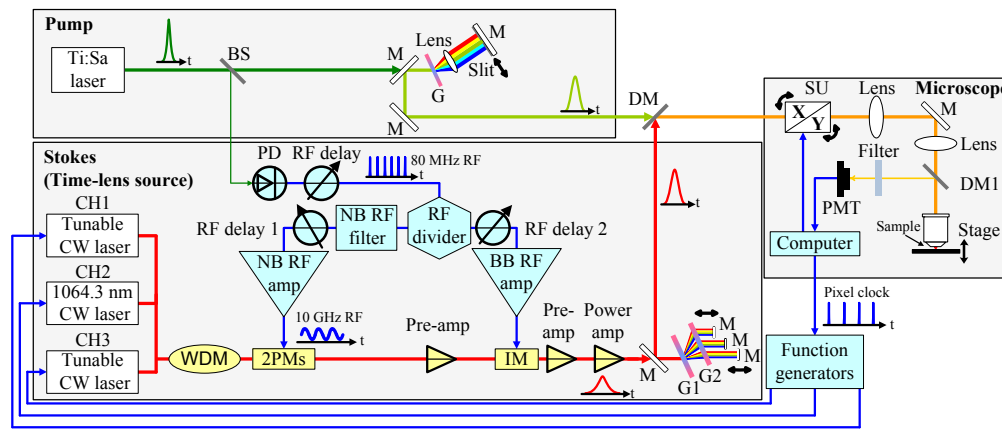

Fig. 1. Experimental setup of a multi-wavelength time-lens source (Stokes), synchronized with a mode-locked Ti:Sa laser (pump). The pump light path is shown in green. The Stokes light path is shown in red, and the electrical path is shown in blue. BS, beam splitter; M, mirror; G, grating (T-1400-800s, 1400 lines/mm, LightSmyth); DM, dichroic mirror (DMLP950R, Thorlabs); PD, photodiode; WDM, wavelength-division multiplexer; NB, narrowband; BB, broadband; PM, phase modulator; IM, intensity modulator; G1, G2, gratings (T-1600-1060s, 1600 lines/mm, LightSmyth); SU, scan unit; DM1, dichroic mirror (FF875-Di01-25 × 36, Semrock); PMT, photomultiplier tube.

The Stokes beam from the time-lens source is spatially combined with the pump beam from the mode-locked Ti:Sa laser by a dichroic mirror. Temporal delay between the two beams is adjusted by tuning the electronically controlled RF delay line, which consists of a discrete electronic delay (PDL-10A, Colby Instruments) with 0.5 ps resolution for coarse adjustment and a continuously tunable RF delay actuated by a linear motor for fine adjustment. The total delay tuning range is approximately 1.2 ns.

For CARS imaging, the spatially and temporally overlapped pump and Stokes beams are sent into a modified laser scanning microscope (FV1000MPE, Olympus), with its scan lens and tube lens changed to match the wavelengths of the pump and Stokes. A 20 × 0.95NA water immersion objective (XLUMPlanFI 20 × /0.95 W, Olympus) is used to focus the beams into the sample. Two telescopes are used to match the beam size with the back-aperture of the objective. The CARS signal is collected in the epi-direction. A dichroic mirror and a bandpass filter (FF01-660/30-25, Semrock, or FBH650-40, Thorlabs, depending on the applications) are used to separate the signal from the excitation beams and other nonlinear signals. The microscope software (FV10-SW, Olympus) controls the scan unit, and displays the signal collected by the microscope's internal photomultiplier tube (PMT). Function generators are used to directly modulate the lasers for the different channels of the time-lens source (see more details in the later sections).

We first characterize the pump, which has a FWHM spectral bandwidth of ~1.8 nm after the pulse shaper. The corresponding FWHM pulse width is ~1 ps, measured by second-order interferometric autocorrelation. The maximum average power of the pump is ~200 mW.
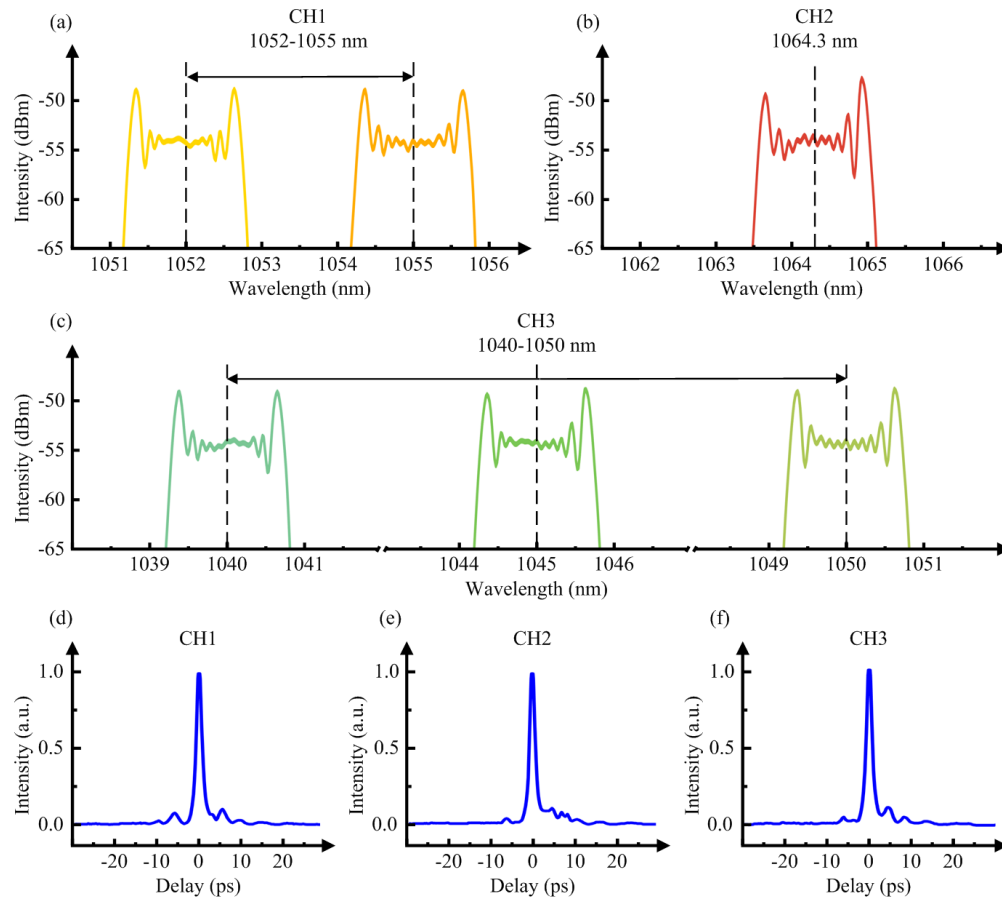
Fig. 2. Characterization of the time-lens source. (a) Wavelength tuning range of CH1 of the time-lens source is 1052-1055 nm. (b) Wavelength of CH2 of the time-lens source is 1064.3 nm. (c) Wavelength tuning range of CH3 of the time-lens source is 1040-1050 nm. For (a), (b) and (c), the spectra after the phase modulation are shown. (d–f) Cross-correlation traces between CH1 (1053.7 nm), CH2 (1064.3 nm), and CH3 (1045.5 nm) of the time-lens source and the spectrally unfiltered 100 fs pulse from the mode-locked Ti:Sa laser.

We then characterize the Stokes pulses. Figure 2(a) shows the wavelength tuning range of CH1 of the time-lens source. The wavelength of the DFB-CW laser is tunable by tuning its operation temperature. Limited by the bandwidth of the WDM, the wavelength tuning range of CH1 is 1052-1055 nm. Figure 2(b) shows the wavelength of CH2, which is 1064.3 nm. Figure 2(c) shows the wavelength tuning range of CH3. Limited by the bandwidth of the WDM, the wavelength tuning range of CH3 is 1040-1050 nm. All channels of the time-lens source have FWHM spectral bandwidth of ~1.5 nm, measured by an optical spectrum analyzer (OSA203C, Thorlabs). For temporal profile characterization, cross-correlation is performed between the output of the time-lens source and the spectrally unfiltered 100 fs pulse from the mode-locked Ti:Sa laser. We use a 0.5-mm thick beta barium borate (β-BBO) crystal for collinear sum frequency generation (SFG). The SFG signal is filtered by a bandpass filter (450-500 nm) and collected by a GaAsP photodiode (G1117, Hamamatsu). The relative delay between the output of the time-lens source and the 100 fs Ti:Sa pulses is

scanned by tuning the RF delay, and the cross-correlation trace is recorded by a DAQ card (USB-9215A, National Instrument). As shown in Figs. 2(d)–2(f), the FWHM pulse width of the time-lens source output is ~1.9 ps for all channels. When only one channel is turned on, the maximum average power is approximately 1.3 W.
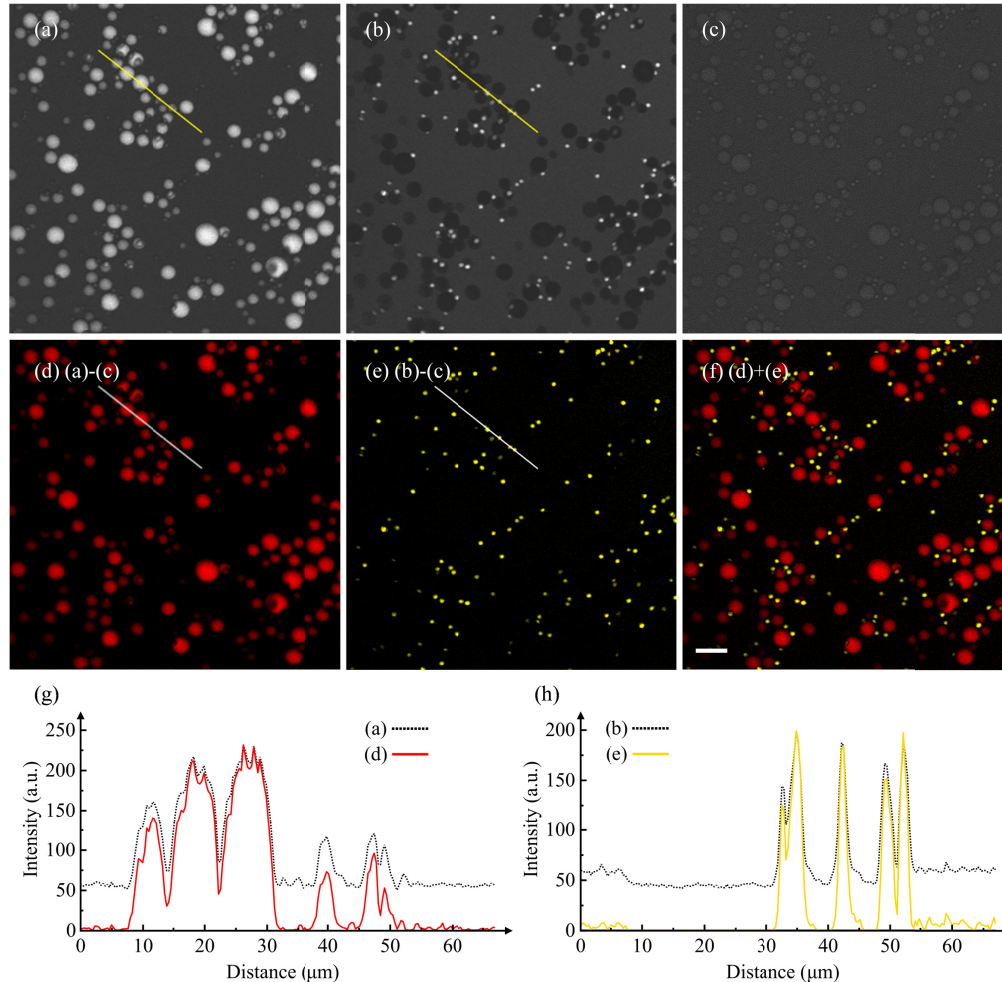

Fig. 3. Two-color CARS imaging of mixed PMMA and PS beads, 512 × 512 pixels, 2 μs/pixel. (a), (b) and (c) are CARS images obtained at Raman frequencies of 2950 cm^{-1}, 3054 cm^{-1}, and 2800 cm^{-1}, respectively. (d–e) Images after subtraction of the nonresonant background of (c) from the CARS signal of (a) and (b), achieving background-free images of PMMA beads (red) and PS beads (yellow). Note that the brightness of (d) and (e) is increased by ~1.5 times to match the brightness scale of (a) and (b). (f) Composite image of PMMA beads (d) and PS beads (e). (g) shows the corresponding intensity profiles along the line indicated in image (a) (dotted black line) and image (d) (solid red line). (h) shows the corresponding intensity profiles along the line indicated in image (b) (dotted black line) and image (e) (solid yellow line). The scale bar is 15 μm.

To show the capability of two-color background-free CARS imaging, we first demonstrate CARS imaging of a mixture of PMMA (4-13 μm diameters) and PS (2.5-3.5 μm diameters) beads immersed in a 2% agarose gel. The wavelength of the pump is tuned to 803.2 nm. The wavelengths of the Stokes are tuned to 1052.6 nm (CH1) and 1064.3 nm (CH2) to probe Raman frequencies at 2950 cm^{-1} and 3054 cm^{-1}, respectively. At the focal plane, the pump, CH1 and CH2 of the Stokes (time-lens source) have the average power of 50 mW, 25 mW

and 25 mW, respectively. As shown in Figs. 3(a) and 3(b), the two-color on-resonance images at 2950 cm^{-1} and 3054 cm^{-1} (obtained separately) have strong resonant signal with noticeable nonresonant background. The nonresonant background is mainly contributed by the surrounding medium. In order to perform background-free imaging, the wavelengths of the pump and CH3 of the Stokes are tuned to 809.1 nm and 1046.1 nm to detect Raman frequency at 2800 cm^{-1}. The average power of pump and Stokes (CH3) are 50 mW and 25 mW, respectively. After subtraction of the off-resonance image Fig. 3(c) from the on-resonance images, two-color background-free CARS images are obtained, as shown in Figs. 3(d) and 3(e). In Fig. 3(d), only PMMA beads (red) contribute to the CARS signal. In Fig. 3(e), only PS beads (yellow) contribute to the CARS signal. The composite of Figs. 3(d) and 3(e) is depicted in Fig. 3(f), which shows spatial distribution of PMMA beads and PS beads. Meanwhile, Figs. 3(g) and 3(h) show that nonresonant background in Figs. 3(a) and 3(b) is effectively suppressed after subtraction. The signal of PMMA beads relative to noise is ~60 at 2950 cm^{-1} in Fig. 3(d), and the signal of PS beads relative to noise is ~40 at 3054 cm^{-1} in Fig. 3(e). The imaging parameters of [34] are similar to ours. By comparing with their data, we conclude that the quality of the images obtained with the time-lens source is at least comparable to that obtained with bulk solid-state lasers.

Figure 3 shows that the system is effective in performing two-color background-free CARS imaging. However, possible artifacts from sample motion is a concern. Thus, we modify the system to achieve simultaneous two-color background-free CARS imaging by synchronizing the time-lens source with the microscope, in order to provide pixel-to-pixel wavelength-switching for the two-color on-resonance imaging and the off-resonance imaging. As shown in Fig. 4(a), the pixel clock of 2 μs period from the microscope is used as the external trigger for three function generators (SDG1032X, Siglent). All the function generators work in N-cycle burst mode, and generate three synchronized rectangular pulse trains. As shown in Fig. 4(b), the period of each pulse train is 6 μs, and the duty cycle is 30%. The delays between different pulse trains can be tuned within a large range (resolution <1 ns). As the lasers for CH1, CH2 and CH3 of the time-lens source are directly modulated by these pulse trains, tuning the relative temporal positions of the three pulse trains can ensure that only one channel is turned on in each pixel dwell time (2 μs), and pixel-to-pixel wavelength-switching is achieved. Thus, different columns of the CARS image correspond to different Raman frequencies, and only one detector (PMT) is needed to collect the CARS signals for the two-color on-resonance imaging and the off-resonance imaging. When the time-lens source works in this mode, each channel of the time-lens source can generate picosecond pulses with the maximum average power of approximately 400 mW.

The capability of simultaneous two-color background-free CARS imaging is demonstrated using excised fresh tissue from a mouse ear. The wavelength of the pump is tuned to 810.7 nm. The wavelengths of the Stokes are tuned to 1053.7 nm (CH1), 1064.3 nm (CH2), and 1045.5 nm (CH3) to probe the Raman peak of CH$_2$ stretching vibration at 2845 cm^{-1}, the Raman peak of CH$_3$ stretching vibration at 2940 cm^{-1}, and the off-resonance background at 2770 cm^{-1}, respectively. At the focal plane, the pump, CH1, CH2 and CH3 of the Stokes (the time-lens source) have the average power of 40 mW, 20 mW, 20 mW and 20 mW, respectively. Figure 4(c) is a CARS image of the fresh tissue from the mouse ear. Figures 4(d) and 4(e) are zoomed-in images from different regions of Fig. 4(c). Zoomed-in illustrations of Figs. 4(d) and 4(e) are shown in Fig. 4(f), showing adjacent pixels obtained at Raman frequencies of 2845 cm^{-1}, 2940 cm^{-1} and 2770 cm^{-1}. Figures 4(g)–4(i) are CARS images extracted from Fig. 4(c), corresponding to Raman frequencies of 2845 cm^{-1}, 2940 cm^{-1} and 2770 cm^{-1}, respectively. As shown in Figs. 4(g) and 4(h), two-color on-resonance images have strong resonant signal with noticeable nonresonant background. The nonresonant background is mainly contributed by the surrounding medium. After subtraction of the off-resonance image Fig. 4(i), two-color background-free CARS images are obtained, as shown in Figs. 4(j) and 4(k). Lipid and protein are main components of mouse ear tissue, and they

both contribute to the CARS signal at 2845 cm^{-1} and 2940 cm^{-1}. The signal of lipid relative to noise is ~50 at 2845 cm^{-1} in Fig. 4(j) and ~30 at 2940 cm^{-1} in Fig. 4(k). We compare our images with those shown in [13,18,35], which has similar imaging parameters to ours. We find that the image quality is comparable. The majority of pixels obtained at 2845 cm^{-1} are brighter than those obtained at 2940 cm^{-1} in possible lipid-rich region of Fig. 4(d), while the majority of pixels obtained at 2940 cm^{-1} are brighter than the ones obtained at 2845 cm^{-1} in possible protein-rich region of Fig. 4(e). These characteristics can also be seen in Figs. 4(j) and 4(k). For example, the first pixel is brighter than the second one in the upper image of Fig. 4(f), while the second pixel is brighter than the first one in the lower image of Fig. 4(f). For the field-of-view shown in Fig. 4(c), each pixel is ~200 nm in the sample plane (Fig. 4(f)), which is sufficiently small so that the three wavelength channels in adjacent pixels sample approximately the same resolution volume.
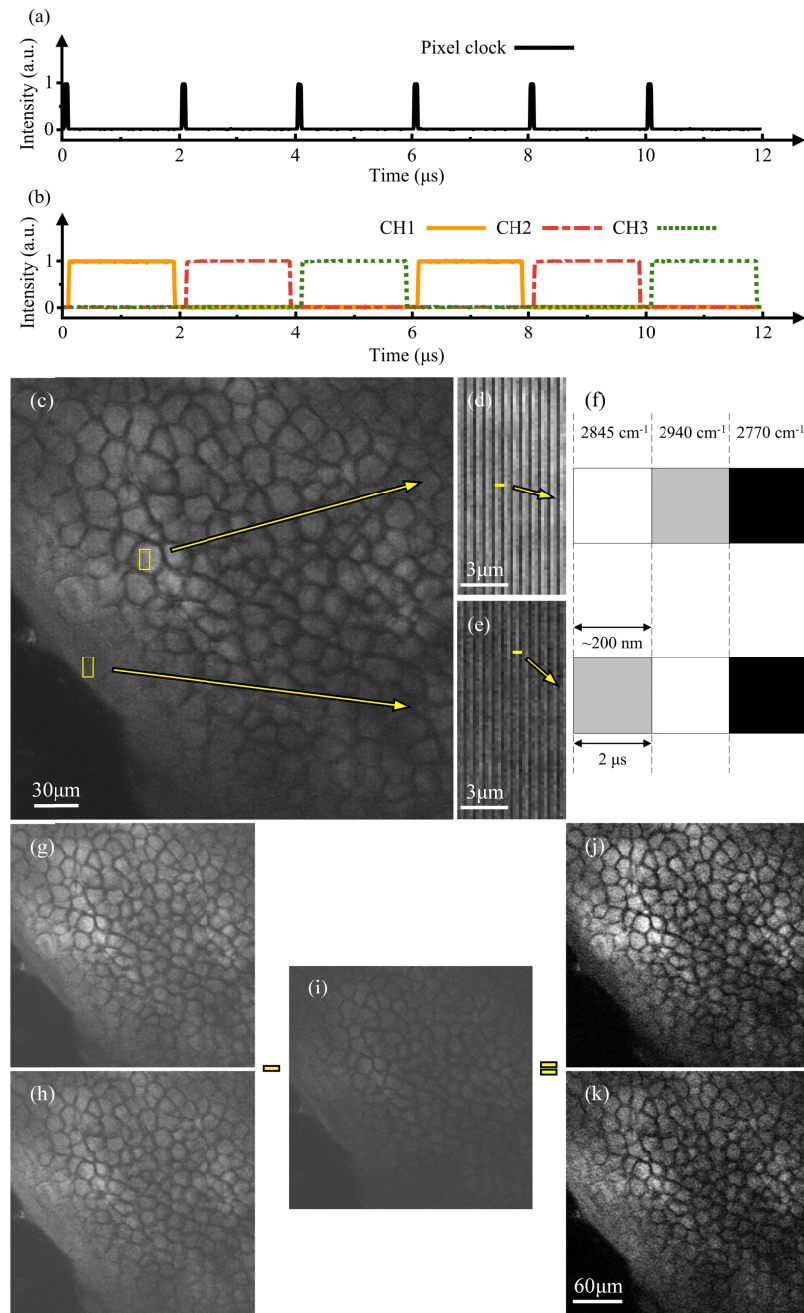
Fig. 4. Demonstration of simultaneous two-color CARS imaging with real-time nonresonant background suppression, 2 μs/pixel, 1536 × 1536 pixels for (c), 512 × 512 pixels for panels (g) to (k). (a) The pixel clock from the microscope. (b) Pulse trains from the function generators. (c) The CARS image of fresh tissue from a mouse ear at depth of 45 μm. Signals of Raman frequencies at 2845 cm⁻¹, 2940 cm⁻¹ and 2770 cm⁻¹ are obtained in different columns of the same image. (d) and (e) are zoomed images from different regions of (c). (f) Zoomed-in views of one column in (d) and (e). (g), (h) and (i) are CARS images, extracted from different columns of (c), corresponding to CH₂ stretching vibration (2845 cm⁻¹), CH₃ stretching vibration (2940 cm⁻¹), and the off-resonance background (2770 cm⁻¹), respectively. (j) and (k) are, respectively, background-free images obtained after subtraction of the nonresonant background of (i) from the CARS signals of (g) and (h).

3. Conclusion

The three-wavelength time-lens source has the advantages of convenient synchronization with any mode-locked laser and microscope pixel clock in a robust, cost-effective, all-fiber configuration. The time-lens source generates three picosecond pulse trains at 1052-1055 nm, 1064.3 nm and 1040-1050 nm, which are synchronized with the mode-locked laser. Function generators externally triggered by the pixel clock from the microscope directly modulate the CW lasers of the three channels of the time-lens source, achieving pixel-to-pixel wavelength-switching, and thus realizing simultaneous two-color CARS imaging with real-time nonresonant background subtraction. The use of the electronic RF delay line to overlap the pump and the Stokes and only one PMT for all three channels greatly simplifies the implementation complexity of multi-color, background-free CARS imaging. The demonstrated time-lens source is analogous to a multi-wavelength telecom transmitter with phase and amplitude modulation, and allows the addition of even more channels with low cost CW lasers and function generators. While not demonstrated in this paper, time-lens sources have been used to perform SRS imaging with high detection sensitivity in our previous work. SRS image of dimethyl sulfoxide (DMSO) in aqueous solution at a concentration down to 28 mM was obtained, with a pixel dwell time of 2 µs [24]. Therefore, CARS imaging with more colors or multiplex SRS imaging could be performed using the time-lens source.

References

1. A. Zumbusch, G. R. Holtom, and X. S. Xie, "Three-dimensional vibrational imaging by coherent anti-Stokes Raman scattering," Phys. Rev. Lett. **82**(20), 4142–4145 (1999).
2. M. Müller and A. Zumbusch, "Coherent anti-Stokes Raman scattering microscopy," ChemPhysChem **8**(15), 2156–2170 (2007).
3. C. W. Freudiger, W. Min, B. G. Saar, S. Lu, G. R. Holtom, C. He, J. C. Tsai, J. X. Kang, and X. S. Xie, "Label-free biomedical imaging with high sensitivity by stimulated Raman scattering microscopy," Science **322**(5909), 1857–1861 (2008).
4. E. O. Potma, D. J. Jones, J.-X. Cheng, X. S. Xie, and J. Ye, "High-sensitivity coherent anti-Stokes Raman scattering microscopy with two tightly synchronized picosecond lasers," Opt. Lett. **27**(13), 1168–1170 (2002).
5. Y. Ozeki, Y. Kitagawa, K. Sumimura, N. Nishizawa, W. Umemura, S. Kajiyama, K. Fukui, and K. Itoh, "Stimulated Raman scattering microscope with shot noise limited sensitivity using subharmonically synchronized laser pulses," Opt. Express **18**(13), 13708–13719 (2010).
6. F. Ganikhanov, S. Carrasco, X. Sunney Xie, M. Katz, W. Seitz, and D. Kopf, "Broadly tunable dual-wavelength light source for coherent anti-Stokes Raman scattering microscopy," Opt. Lett. **31**(9), 1292–1294 (2006).
7. K. Kieu, B. G. Saar, G. R. Holtom, X. S. Xie, and F. W. Wise, "High-power picosecond fiber source for coherent Raman microscopy," Opt. Lett. **34**(13), 2051–2053 (2009).
8. A. F. Pegoraro, A. Ridsdale, D. J. Moffatt, Y. Jia, J. P. Pezacki, and A. Stolow, "Optimally chirped multimodal CARS microscopy based on a single Ti:sapphire oscillator," Opt. Express **17**(4), 2984–2996 (2009).
9. A. F. Pegoraro, A. Ridsdale, D. J. Moffatt, J. P. Pezacki, B. K. Thomas, L. Fu, L. Dong, M. E. Fermann, and A. Stolow, "All-fiber CARS microscopy of live cells," Opt. Express **17**(23), 20700–20706 (2009).
10. G. Krauss, T. Hanke, A. Sell, D. Träutlein, A. Leitenstorfer, R. Selm, M. Winterhalder, and A. Zumbusch, "Compact coherent anti-Stokes Raman scattering microscope based on a picosecond two-color Er:fiber laser system," Opt. Lett. **34**(18), 2847–2849 (2009).
11. A. Gambetta, V. Kumar, G. Grancini, D. Polli, R. Ramponi, G. Cerullo, and M. Marangoni, "Fiber-format stimulated-Raman-scattering microscopy from a single laser oscillator," Opt. Lett. **35**(2), 226–228 (2010).
12. M. Baumgartl, M. Chemnitz, C. Jauregui, T. Meyer, B. Dietzek, J. Popp, J. Limpert, and A. Tünnermann, "All-fiber laser source for CARS microscopy based on fiber optical parametric frequency conversion," Opt. Express **20**(4), 4484–4493 (2012).

13. S. Lefrancois, D. Fu, G. R. Holtom, L. Kong, W. J. Wadsworth, P. Schneider, R. Herda, A. Zach, X. Sunney Xie, and F. W. Wise, "Fiber four-wave mixing source for coherent anti-Stokes Raman scattering microscopy," Opt. Lett. **37**(10), 1652–1654 (2012).
14. S. Yue, M. N. Slipchenko, and J.-X. Cheng, "Multimodal nonlinear optical microscopy," Laser Photonics Rev. **5**(4), 496–512 (2011).
15. F. Lu, W. Zheng, C. Sheppard, and Z. Huang, "Interferometric polarization coherent anti-Stokes Raman scattering (IP-CARS) microscopy," Opt. Lett. **33**(6), 602–604 (2008).
16. Y. J. Lee and M. T. Cicerone, "Vibrational dephasing time imaging by time-resolved broadband coherent anti-Stokes Raman scattering microscopy," Appl. Phys. Lett. **92**(4), 041108 (2008).
17. B.-C. Chen, J. Sung, and S.-H. Lim, "Chemical imaging with frequency modulation coherent anti-Stokes Raman scattering microscopy at the vibrational fingerprint region," J. Phys. Chem. B **114**(50), 16871–16880 (2010).
18. B.-C. Chen, J. Sung, X. Wu, and S.-H. Lim, "Chemical imaging and microspectroscopy with spectral focusing coherent anti-Stokes Raman scattering," J. Biomed. Opt. **16**(2), 021112 (2011).
19. C. L. Evans, E. O. Potma, and X. S. Xie, "Coherent anti-stokes raman scattering spectral interferometry: determination of the real and imaginary components of nonlinear susceptibility χ(3) for vibrational microscopy," Opt. Lett. **29**(24), 2923–2925 (2004).
20. K. Chen, T. Wu, H. Wei, T. Zhou, and Y. Li, "Quantitative chemical imaging with background-free multiplex coherent anti-Stokes Raman scattering by dual-soliton Stokes pulses," Biomed. Opt. Express **7**(10), 3927–3939 (2016).
21. M. Duncan, J. Reintjes, and T. Manuccia, "Imaging biological compounds using the coherent anti-Stokes Raman scattering microscope," Opt. Eng. **24**(2), 242352 (1985).
22. K. Wang, C. W. Freudiger, J. H. Lee, B. G. Saar, X. S. Xie, and C. Xu, "Synchronized time-lens source for coherent Raman scattering microscopy," Opt. Express **18**(23), 24019–24024 (2010).
23. K. Wang and C. Xu, "Fiber-delivered picosecond source for coherent Raman scattering imaging," Opt. Lett. **36**(21), 4233–4235 (2011).
24. K. Wang, D. Zhang, K. Charan, M. N. Slipchenko, P. Wang, C. Xu, and J.-X. Cheng, "Time-lens based hyperspectral stimulated Raman scattering imaging and quantitative spectral analysis," J. Biophotonics **6**(10), 815–820 (2013).
25. B. Li, K. Charan, K. Wang, T. Rojo, D. Sinefeld, and C. Xu, "Nonresonant background suppression for coherent anti-Stokes Raman scattering microscopy using a multi-wavelength time-lens source," Opt. Express **24**(23), 26687–26695 (2016).
26. B. H. Kolner, "Space-time duality and the theory of temporal imaging," IEEE J. Quantum Electron. **30**(8), 1951–1963 (1994).
27. J. van Howe, J. Hansryd, and C. Xu, "Multiwavelength pulse generator using time-lens compression," Opt. Lett. **29**(13), 1470–1472 (2004).
28. J. van Howe and C. Xu, "Ultrafast optical delay line by use of a time-prism pair," Opt. Lett. **30**(1), 99–101 (2005).
29. J. van Howe and C. Xu, "Ultrafast optical delay line using soliton propagation between a time-prism pair," Opt. Express **13**(4), 1138–1143 (2005).
30. Z. Jiang, D. E. Leaird, and A. M. Weiner, "Optical processing based on spectral line-by-line pulse shaping on a phase-modulated CW laser," IEEE J. Quantum Electron. **42**(7), 657–665 (2006).
31. J. van Howe and C. Xu, "Ultrafast optical signal processing based upon space-time dualities," J. Lightwave Technol. **24**(7), 2649–2662 (2006).
32. J. van Howe, J. H. Lee, and C. Xu, "Generation of 3.5 nJ femtosecond pulses from a continuous-wave laser without mode locking," Opt. Lett. **32**(11), 1408–1410 (2007).
33. D. H. Broaddus, M. A. Foster, O. Kuzucu, A. C. Turner-Foster, K. W. Koch, M. Lipson, and A. L. Gaeta, "Temporal-imaging system with simple external-clock triggering," Opt. Express **18**(13), 14262–14269 (2010).
34. F.-K. Lu, M. Ji, D. Fu, X. Ni, C. W. Freudiger, G. Holtom, and X. S. Xie, "Multicolor stimulated Raman scattering (SRS) microscopy," Mol. Phys. **110**(15-16), 1927–1932 (2012).
35. M. Andreana, T. Le, A. K. Hansen, A. J. Verhoef, O. B. Jensen, P. E. Andersen, P. Slezak, W. Drexler, A. Fernández, and A. Unterhubera, "Epi-detecting label-free multimodal imaging platform using a compact diode-pumped femtosecond solid-state laser," J. Biomed. Opt. **22**(9), 091517 (2017).